

## GENERALIZED PLANE STRAIN THERMOPIEZOELECTRIC ANALYSIS OF MULTILAYERED PLATES

**Senthil S. Vel**

*Department of Mechanical Engineering  
University of Maine  
Orono, Maine, USA*

**R. C. Batra**

*Department of Engineering Science and Mechanics  
Virginia Polytechnic Institute and State University  
Blacksburg, Virginia, USA*

*The generalized plane strain thermopiezoelectric deformations of laminated thick plates are analyzed using the Eshelby–Stroh formalism. The laminated plate consists of homogeneous laminae of arbitrary thicknesses. The three-dimensional equations of linear anisotropic thermopiezoelectricity simplified to the case of generalized plane strain deformations are exactly satisfied at every point in the body. The analytical solution is in terms of an infinite series. The continuity conditions at the interfaces and boundary conditions at the top and bottom surfaces and edges are used to determine coefficients in the series. The formulation admits different thermal, electrical, and mechanical boundary conditions at the edges of each lamina and is applicable to thick and thin laminated plates. Laminated plates containing piezoelectric laminae poled either in the thickness direction or in the axial direction are analyzed, and results are presented for plates with edges either rigidly clamped, simply supported, or traction-free.*

Smart structures, consisting of piezoelectric materials integrated with structural systems, have found widespread use in engineering applications. Piezoelectric materials are capable of altering the structure's response through sensing, actuation, and control. They exhibit two basic electromechanical phenomena that have led to their use as sensors and actuators in the control of structural systems. In sensor applications, an applied mechanical strain induces an electric potential in the material due to the direct piezoelectric effect; whereas in actuator applications, an applied electric field causes the material to deform. Of the 21 crystal classes that

Received 22 April 2002; accepted 19 June 2002.

R. C. Batra's work was partially supported by the ONR grant N00014-98-1-0300 of Virginia Polytechnic Institute and State University.

Address correspondence to Senthil S. Vel, Department of Mechanical Engineering, University of Maine, 5711 Boardman Hall, Room 214, Orono, ME 04469. E-mail: vel@umeme.maine.edu

exhibit the piezoelectric effect, 10 also show the pyroelectric effect, i.e., a temperature change produces an electric potential in the material. It is also observed that a piezocomposite comprised of piezoceramic inclusions embedded in an elastic matrix exhibits pyroelectric effect even when none of the constituents are pyroelectric; for example, see Dunn [1] and Jiang and Batra [2].

Thermal effects greatly influence the performance of piezoelectric actuators and sensors, especially when they are required to operate in severe temperature environments. The governing equations of a thermopiezoelectric material—where the mechanical, electrical, and thermal fields are coupled—have been derived by Mindlin [3]. General theorems of thermopiezoelectricity are given in Nowacki [4] and Iesan [5]. Huang and Batra [6] and Yang [7] developed equations governing deformations of piezothermoviscoelectric materials.

Tauchert [8] and Jonnalagadda et al. [9] developed plate theories for thermopiezoelectric laminated plates. Finite element studies of thermopiezoelectric laminated structures have been carried out by Rao and Sunar [10] and Tzou and Ye [11]. Tang et al. [12] assessed the accuracy of various thermopiezoelectric plate models. Lee and Saravanos [13] developed a coupled, layerwise theory to analyze the thermopiezoelectric behavior of composite structures. Ishihara and Noda [14] studied thermopiezoelectric laminates including the effects of transverse shear deformation and coupling. Due to the coupling of the mechanical, electrical, and thermal fields and its inherent anisotropy, the analysis of thermopiezoelectric materials is a challenging task and relatively few analytical solutions to the three-dimensional governing equations are available in the literature. They are mainly confined to orthorhombic thermopiezoelectric plates whose edges are simply supported. Analytical solutions to the cylindrical bending of simply supported laminated plates were provided by Dube et al. [15, 16], Kapuria et al. [17], and Shang et al. [18]. Xu et al. [19] and Tang and Xu [20] obtained an analytical solution to the coupled three-dimensional thermopiezoelectricity equations for laminated rectangular plates. A three-dimensional transient analysis of thermopiezoelectric composite plates was carried out by Ootao and Tanigawa [21]. Cheng and Batra [22] used a three-dimensional asymptotic scheme to analyze thermopiezoelectric laminates. Ashida and Tauchert [23] derived solutions for circular thermopiezoelectric plates having arbitrary edge conditions using potential functions. Yang and Batra [24] analyzed the damping introduced by heat conduction in steady-state vibrations of a thermopiezoelectric plate. A review of the recent developments in thermopiezoelectricity with relevance to smart structures was presented by Tauchert et al. [25].

The Eshelby–Stroh formalism [26–28] provides exact solutions of governing equations of anisotropic elasticity under generalized plane strain deformations in terms of analytic functions. Vel and Batra [29, 30] expressed the analytic functions in the form of an infinite series to study the generalized plane strain deformations of laminated piezoelectric and thermoelastic plates subjected to arbitrary boundary conditions. Here, the method is extended to thermopiezoelectric problems. The mechanical equilibrium, charge equilibrium, and steady-state heat conduction equations are exactly satisfied at every point in the domain, and various constants in the general solution are determined from the boundary conditions at the bound-

ing surfaces and continuity conditions at the interfaces between adjoining laminae. This results in an infinite system of linear equations in infinitely many unknowns. By retaining a large number of terms in the series, the solution can be computed to any desired degree of accuracy. The formulation admits different mechanical, electrical, and thermal boundary conditions at the edges of each lamina and is applicable to thick and thin laminated plates. The procedure is illustrated by computing results for the generalized plane strain deformation of thick laminated plates containing either thickness poled or axially poled piezoelectric laminae.

**FORMULATION OF THE PROBLEM**

We use a rectangular Cartesian coordinate system, shown in Figure 1, to describe the infinitesimal quasi-static deformations of a thermopiezoelectric laminate occupying the region  $[0, L_1] \times (-\infty, \infty) \times [L_3^{(1)}, L_3^{(N+1)}]$  in the unstressed reference configuration. Planes  $x_3 = L_3^{(1)}, \dots, L_3^{(n)}, \dots, L_3^{(N+1)}$  describe the lower bounding surface, the horizontal interfaces between adjoining laminae, and the top bounding surface.

The equilibrium equations in the absence of body forces, free charges, and heat sources are [31]

$$\sigma_{ij,j} = 0 \quad D_{i,i} = 0 \quad q_{i,i} = 0 \quad (i, j = 1, 2, 3) \tag{1}$$

where  $\sigma_{ij}$  is the Cauchy stress tensor,  $D_i$  the electric displacement vector, and  $q_i$  the heat flux vector. A comma followed by index  $j$  indicates partial differentiation with respect to the position  $x_j$  of a material particle, and a repeated index implies summation over the range of the index.

The constitutive equations of a linear thermopiezoelectric medium are [31]

$$\begin{aligned} \sigma_{ij} &= C_{ijkl}\epsilon_{kl} - e_{kij}E_k - \beta_{ij}T \\ D_i &= e_{ikl}\epsilon_{kl} + \varepsilon_{ik}E_k + r_iT \\ q_i &= -\kappa_{ij}T_{,j} \end{aligned} \tag{2}$$

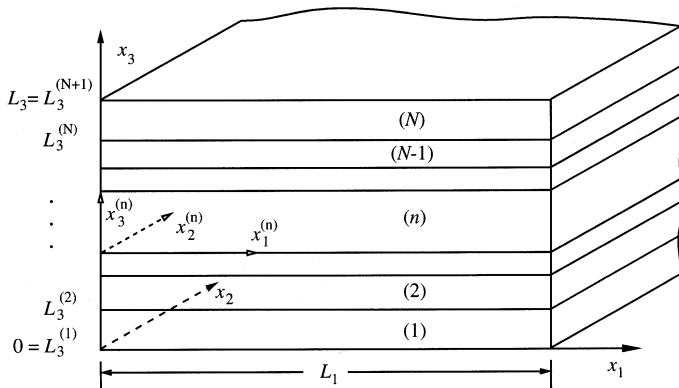


Figure 1. An  $N$ -layer laminated piezoelectric plate.

where  $\epsilon_{kl}$  is the infinitesimal strain tensor,  $E_k$  the electric field vector,  $T$  the temperature rise of a material particle from that in the stress-free reference configuration,  $C_{ijkl}$  the isothermal elastic moduli,  $e_{kij}$  the piezoelectric coefficients,  $\beta_{ij}$  the stress-temperature coefficients,  $\epsilon_{ik}$  the permittivities,  $r_i$  the pyroelectric coefficients, and  $\kappa_{ij}$  the thermal conductivities. We will interchangeably use the direct and the indicial notation. The infinitesimal strain tensor and the electric field vector are related to the mechanical displacement vector  $u_k$  and the electric potential  $\phi$  by

$$\epsilon_{kl} = \frac{1}{2}(u_{k,l} + u_{l,k}) \quad E_k = -\phi_{,k} \tag{3}$$

The material constants are assumed to satisfy the following symmetries:

$$C_{ijkl} = C_{jikl} = C_{klij} \quad e_{kij} = e_{kji} \quad \beta_{ij} = \beta_{ji} \quad \epsilon_{ik} = \epsilon_{ki} \quad \kappa_{ij} = \kappa_{ji} \tag{4}$$

Furthermore, the elasticity tensor, the permittivity tensor, and the thermal conductivity tensor are assumed to be positive definite. In the most general case, there are 21 independent elastic moduli, 18 independent piezoelectric coefficients, 6 independent permittivities, 6 independent stress-temperature coefficients, 3 independent pyroelectric coefficients, and 6 independent thermal conductivities.

On the edges  $x_1 = 0, L_1$  and on the top and the bottom surfaces  $x_3 = 0, L_3$ , the displacement or traction components, and the electric potential or the normal component of the electric displacement are specified as

$$\begin{aligned} \mathbf{I}_{u\phi}^{(s)} \begin{bmatrix} \mathbf{u} \\ \phi \end{bmatrix} + \mathbf{I}_{\sigma D}^{(s)} \begin{bmatrix} \boldsymbol{\sigma}_s \\ D_s \end{bmatrix} &= \mathbf{f}^{(s)} \quad \text{on } x_s = 0 \\ \mathbf{J}_{u\phi}^{(s)} \begin{bmatrix} \mathbf{u} \\ \phi \end{bmatrix} + \mathbf{J}_{\sigma D}^{(s)} \begin{bmatrix} \boldsymbol{\sigma}_s \\ D_s \end{bmatrix} &= \mathbf{g}^{(s)} \quad \text{on } x_s = L_s \quad (s = 1, 3) \end{aligned} \tag{5}$$

where  $(\boldsymbol{\sigma}_k)_i = \sigma_{ik}$ ;  $\mathbf{I}_{u\phi}^{(s)}$ ,  $\mathbf{I}_{\sigma D}^{(s)}$ ,  $\mathbf{J}_{u\phi}^{(s)}$ , and  $\mathbf{J}_{\sigma D}^{(s)}$  are  $4 \times 4$  diagonal matrices; and  $\mathbf{f}^{(s)}$  and  $\mathbf{g}^{(s)}$  are known vector functions. For ideal restraints at the edges, these diagonal matrices have entries of either zero or one such that

$$\mathbf{I}_{u\phi}^{(s)} + \mathbf{I}_{\sigma D}^{(s)} = \mathbf{J}_{u\phi}^{(s)} + \mathbf{J}_{\sigma D}^{(s)} = \mathbf{I}$$

with  $\mathbf{I}$  being the  $4 \times 4$  identity matrix. In other words, we specify either a component of the displacement or of the traction vector in each coordinate direction at every point on the boundary. For ideal restraints at the edges, if the surface  $x_1 = 0$  is rigidly clamped and electrically grounded, then  $\mathbf{I}_{u\phi}^{(1)} = \mathbf{I}$ ,  $\mathbf{I}_{\sigma D}^{(1)} = \mathbf{0}$ , and  $\mathbf{f}^{(1)} = \mathbf{0}$ , that is,  $u_1 = u_2 = u_3 = 0$  and  $\phi = 0$ . If the edge is simply supported and the normal component of the electric displacement is zero (the surface is free of electric charge), then  $\mathbf{I}_{u\phi}^{(1)} = \text{diag}[0, 0, 1, 0]$ ,  $\mathbf{I}_{\sigma D}^{(1)} = \text{diag}[1, 1, 0, 1]$ , and  $\mathbf{f}^{(1)} = \mathbf{0}$ . Boundary conditions for a traction-free and electrically grounded edge can be specified as

$\mathbf{I}_{u\phi}^{(1)} = \text{diag}[0, 0, 0, 1]$ ,  $\mathbf{I}_{\sigma D}^{(1)} = \text{diag}[1, 1, 1, 0]$ , and  $\mathbf{f}^{(1)} = \mathbf{0}$ . The thermal boundary conditions are specified as

$$\begin{aligned} m^{(s)}T + r^{(s)}q_s &= \varphi^{(s)} \quad \text{on } x_s = 0 \\ \tilde{m}^{(s)}T + \tilde{r}^{(s)}q_s &= \tilde{\varphi}^{(s)} \quad \text{on } x_s = L_s \quad (s = 1, 3) \end{aligned} \tag{6}$$

By appropriately choosing  $m^{(s)}$ ,  $r^{(s)}$ ,  $\tilde{m}^{(s)}$ , and  $\tilde{r}^{(s)}$  in these equations, various thermal boundary conditions corresponding to a prescribed temperature, a prescribed heat flux, or exposure to an ambient temperature through a boundary conductance can be specified.

The interface continuity conditions on the material surface  $x_3 = H^{(n)}$  between adjoining laminae may be specified as follows:

- i. We assume that the two adjoining laminae are perfectly bonded together. Thus, at their common interface, the displacements, surface tractions, electric potential, the normal component of the electric displacement, the temperature, and the normal component of the heat flux vector between the adjoining laminae are taken to be continuous. That is,

$$[[\mathbf{u}]] = \mathbf{0} \quad [[\boldsymbol{\sigma}_3]] = \mathbf{0} \quad [[\phi]] = 0 \quad [[D_3]] = 0 \quad [[T]] = 0 \quad [[q_3]] = 0 \quad \text{on } x_3 = H^{(n)} \tag{7}$$

Here  $[[\mathbf{u}]]$  denotes the jump in the value of  $\mathbf{u}$  across an interface.

- ii. If the surface  $x_3 = H^{(n)}$  is an electroded interface between two adjoining layers, then the electric potential on this surface is a known function  $\gamma(x_1)$  while the normal component of the electric displacement need not be continuous across the interface, that is,

$$[[\mathbf{u}]] = \mathbf{0} \quad [[\boldsymbol{\sigma}_3]] = \mathbf{0} \quad \phi = \gamma(x_1) \quad [[T]] = 0 \quad [[q_3]] = 0 \quad \text{on } x_3 = H^{(n)} \tag{8}$$

Since the applied loads are independent of  $x_2$ , the body is of infinite extent in the  $x_2$ -direction, and material properties are uniform, we postulate that the displacement vector  $\mathbf{u}$ , the electric potential  $\phi$ , and the temperature change  $T$  are functions of  $x_1$  and  $x_3$  only. Thus deformations of the laminate correspond to a generalized plane state of deformation.

### SOLUTION OF THE PROBLEM

We extend the Eshelby–Stroh [26, 27] formalism as described by Ting [28] to obtain a general solution of Eqs. (1) and (2). Boundary conditions (5) and (6), and interface conditions (7) or (8), will be used to find constants in the general solution. We construct a local coordinate system  $x_1^{(n)}, x_2^{(n)}, x_3^{(n)}$  with origin at the point where the global  $x_3$ -axis intersects the bottom surface of the  $n$ th lamina; the local axes are parallel to the global axes (Figure 1). The thickness of the  $n$ th lamina is denoted by  $h^{(n)} = L_3^{(n+1)} - L_3^{(n)}$ .

### A General Solution

In deriving a general solution of Eqs. (1) and (2) for the  $n$ th lamina, we drop the superscript  $n$  for convenience, it being understood that all material properties and variables belong to this lamina. Assume that

$$\begin{bmatrix} \mathbf{u} \\ \phi \end{bmatrix} = \mathbf{a}f(z) + \mathbf{c}g(z_\tau) \quad T = g'(z_\tau) \tag{9}$$

where

$$z = x_1 + px_3 \quad z_\tau = x_1 + \tau x_3$$

$f$  and  $g$  are arbitrary analytic functions of their arguments, and  $\mathbf{a}, \mathbf{c}, p$ , and  $\tau$  are possible complex constants to be determined. Substituting Eqs. (9) and (3) into Eq. (2) and the result into Eq. (1) gives

$$\begin{aligned} \mathbf{D}(p)\mathbf{a} &= \mathbf{0} \\ \mathbf{D}(p)\mathbf{c} &= \widehat{\boldsymbol{\beta}}_1 + \tau\widehat{\boldsymbol{\beta}}_3 \\ \kappa_{33}\tau^2 + (\kappa_{13} + \kappa_{31})\tau + \kappa_{11} &= 0 \end{aligned} \tag{10}$$

where

$$\begin{aligned} \mathbf{D}(p) &= \mathbf{Q} + p(\mathbf{R} + \mathbf{R}^T) + p^2\mathbf{T} \\ \mathbf{Q} &= \begin{bmatrix} \mathbf{Q}^E & \mathbf{e}_{11} \\ \mathbf{e}_{11}^T & -\varepsilon_{11} \end{bmatrix} \quad \mathbf{R} = \begin{bmatrix} \mathbf{R}^E & \mathbf{e}_{31} \\ \mathbf{e}_{13}^T & -\varepsilon_{13} \end{bmatrix} \quad \mathbf{T} = \begin{bmatrix} \mathbf{T}^E & \mathbf{e}_{33} \\ \mathbf{e}_{33}^T & -\varepsilon_{33} \end{bmatrix} \\ Q_{ik}^E &= C_{i1k1} \quad R_{ik}^E = C_{i1k3} \quad T_{ik}^E = C_{i3k3} \\ (\mathbf{e}_{ij})_k &= e_{ijk} \quad (\boldsymbol{\beta}_k)_i = \beta_{ik} \quad \widehat{\boldsymbol{\beta}}_k = \begin{bmatrix} \boldsymbol{\beta}_k \\ -r_k \end{bmatrix} \end{aligned} \tag{11}$$

The eigenvalue  $\tau$  depends on the components of the thermal conductivity tensor and satisfies the quadratic equation (10)<sub>3</sub>. Since  $\kappa_{ij}$  is positive definite,  $\tau$  obtained by solving Eq. (10)<sub>3</sub> cannot be real [28, 32]. We denote the root with positive imaginary part by  $\tau$  and its complex conjugate by  $\bar{\tau}$ . The eigenvalues  $p$  and their associated eigenvectors  $\mathbf{a}$  are obtained by solving the eigenvalue problem (10)<sub>1</sub>. Since  $C_{jmqr}$  and  $\varepsilon_{jm}$  are positive definite,  $p$  cannot be real [28, 33]. Therefore, there are four pairs of complex conjugates for  $p$ . Let

$$\text{Im}(p_\alpha) > 0 \quad p_{\alpha+4} = \bar{p}_\alpha \quad \mathbf{a}_{\alpha+4} = \bar{\mathbf{a}}_\alpha \quad (\alpha = 1, 2, 3, 4) \tag{12}$$

The vector  $\mathbf{c}$  associated with the thermal eigenvalue  $\tau$  is obtained by solving the system of equations (10)<sub>2</sub>. If the eigenvalues  $p_\alpha$  and  $\tau$  are distinct, a general solution of Eqs. (1) and (2) obtained by superposing solutions of the form (9) is

$$\begin{aligned} \begin{bmatrix} \mathbf{u} \\ \phi \end{bmatrix} &= \sum_{\alpha=1}^4 [\mathbf{a}_\alpha f_\alpha(z_\alpha) + \bar{\mathbf{a}}_\alpha f_{\alpha+4}(\bar{z}_\alpha)] + \mathbf{c} g_1(z_\tau) + \bar{\mathbf{c}} g_2(\bar{z}_\tau) \\ T &= g'_1(z_\tau) + g'_2(\bar{z}_\tau) \end{aligned} \tag{13}$$

where  $f_\alpha$  ( $\alpha = 1, 2, \dots, 8$ ),  $g_1$  and  $g_2$  are arbitrary analytic functions,  $z_\alpha = x_1 + p_\alpha x_3$ , and  $g'(z) = dg(z)/dz$ . Substituting Eq. (13) into Eq. (2) yields

$$\begin{aligned} \begin{bmatrix} \sigma_1 \\ D_1 \end{bmatrix} &= \sum_{\alpha=1}^4 [-p_\alpha \mathbf{b}_\alpha f'_\alpha(z_\alpha) - \bar{p}_\alpha \bar{\mathbf{b}}_\alpha f'_{\alpha+4}(\bar{z}_\alpha)] - \tau \mathbf{d} g'_1(z_\tau) - \bar{\tau} \bar{\mathbf{d}} g'_2(\bar{z}_\tau) \\ \begin{bmatrix} \sigma_3 \\ D_3 \end{bmatrix} &= \sum_{\alpha=1}^4 [\mathbf{b}_\alpha f'_\alpha(z_\alpha) + \bar{\mathbf{b}}_\alpha f'_{\alpha+4}(\bar{z}_\alpha)] + \mathbf{d} g'_1(z_\tau) + \bar{\mathbf{d}} g'_2(\bar{z}_\tau) \\ \mathbf{q} &= -(\kappa_1 + \tau \kappa_3) g''_1(z_\tau) - (\kappa_1 + \bar{\tau} \kappa_3) g''_2(\bar{z}_\tau) \end{aligned} \tag{14}$$

where

$$\mathbf{b}_\alpha = (\mathbf{R}^T + p_\alpha \mathbf{T}) \mathbf{a}_\alpha \quad \mathbf{d} = (\mathbf{R}^T + \tau \mathbf{T}) \mathbf{c} - \hat{\boldsymbol{\beta}}_3 \quad (\boldsymbol{\kappa}_m)_j = \kappa_{jm}$$

The general solution (13) and (14) is applicable when (i) there exist four independent eigenvectors  $\mathbf{a}_\alpha$  even when the eigenvalues  $p_\alpha$  ( $\alpha = 1, \dots, 4$ ) are not distinct and (ii) either  $\tau$  is not equal to one of the  $p$ 's or if  $\tau = p$ , then Eq. (10)<sub>2</sub> can be solved for  $\mathbf{c}$ . Materials that do not satisfy these conditions are *degenerate thermopiezoelectric materials*. Wu [34] and Yang et al. [35] described the procedure by which the general solution for degenerate materials can be constructed. Consider a degenerate material for which  $p_1 = p_2 \neq p_3 \neq p_4$ ,  $\tau \neq p_\alpha$ , and there is only one eigenvector  $\mathbf{a}_1$  associated with the double root  $p_1$ . A second independent solution associated with the eigenvalue  $p_1$  is

$$\mathbf{u} = \frac{d}{dp_1} [\mathbf{a}_1 f_2(z_1)] = \frac{d\mathbf{a}_1}{dp_1} f_2(z_1) + \mathbf{a}_1 \frac{df_2(z_1)}{dp_1} \tag{15}$$

Here  $d\mathbf{a}_1/dp_1$  is obtained by differentiating Eq. (10)<sub>1</sub>,

$$\mathbf{D} \frac{d\mathbf{a}_1}{dp_1} + \frac{d\mathbf{D}}{dp_1} \mathbf{a}_1 = \mathbf{0} \tag{16}$$

Dempsey and Sinclair [36] proved the existence of a nontrivial solution for  $\mathbf{a}_1$  and  $d\mathbf{a}_1/dp_1$  of Eqs. (10)<sub>1</sub> and (16). Therefore, the general solution is

$$\begin{aligned} \mathbf{u} &= \sum_{\alpha=1}^4 [\mathbf{a}_\alpha f_\alpha(z_\alpha) + \bar{\mathbf{a}}_\alpha f_{\alpha+4}(\bar{z}_\alpha)] + \mathbf{a}_1 \frac{df_2(z_1)}{dp_1} + \bar{\mathbf{a}}_1 \frac{df_5(\bar{z}_1)}{d\bar{p}_1} + \mathbf{c} g_1(z_\tau) + \bar{\mathbf{c}} g_2(\bar{z}_\tau) \\ T &= g'_1(z_\tau) + g'_2(\bar{z}_\tau) \end{aligned} \tag{17}$$

where  $\mathbf{a}_2 = d\mathbf{a}_1/dp_1$ . The corresponding general solution for the stress tensor and the heat flux is obtained by substituting Eq. (17) into Eq. (2). It is important to note that, regardless of whether the material is degenerate or not, there are 10 arbitrary analytic functions, namely  $f_\alpha$  ( $\alpha = 1, \dots, 8$ ),  $g_1$ , and  $g_2$ . Our treatment of the degenerate case differs from that of Wu [34] and Yang et al. [35] only in one aspect, namely, we do not require  $f_2(z_1) = f_1(z_1)$  as they do.

### A Series Solution

Even though Eq. (13) satisfies the equilibrium equations (1) for any analytic functions  $f_\alpha, g_1$ , and  $g_2$ , a choice based on the geometry of the problem and boundary conditions can reduce the algebraic work involved. We select for the  $n$ th lamina

$$\begin{aligned}
 f_\alpha(z_\alpha) &= \sum_{m=0}^{\infty} \{v_{m\alpha}^{(1)} \exp(\eta_{m\alpha} z_\alpha) + w_{m\alpha}^{(1)} \exp(\eta_{m\alpha}(l - z_\alpha))\} \\
 &\quad + \sum_{k=0}^{\infty} \{v_{k\alpha}^{(3)} \exp(\lambda_{k\alpha} z_\alpha) + w_{k\alpha}^{(3)} \exp(\lambda_{k\alpha}(p_\alpha h - z_\alpha))\} \\
 f_{\alpha+4}(\bar{z}_\alpha) &= \overline{f_\alpha(z_\alpha)} \quad (\alpha = 1, 2, 3, 4)
 \end{aligned}
 \tag{18}$$

where  $0 \leq x_1 \leq L_1, 0 \leq x_3 \leq h$ ,

$$\eta_{m\alpha} = \begin{cases} \frac{-m_0\pi i}{p_\alpha h} & \text{if } m = 0 \\ -\frac{m\pi i}{p_\alpha h} & \text{if } m \geq 1 \end{cases} \quad \lambda_{k\alpha} = \begin{cases} \frac{k_0\pi i}{L_1} & \text{if } k = 0 \\ \frac{k\pi i}{L_1} & \text{if } k \geq 1 \end{cases}
 \tag{19}$$

and  $m_0, k_0 \in (0, 1)$ . The functions involving  $m_0$  and  $k_0$  play the role of the constant term in a Fourier series expansion. The functions  $g_1$  and  $g_2$  are chosen as

$$\begin{aligned}
 g_1(z_\tau) &= \sum_{m=0}^{\infty} \{\hat{v}_m^{(1)} \exp(\xi_m z_\tau) + \hat{w}_m^{(1)} \exp(\xi_m(l - z_\tau))\} \\
 &\quad + \sum_{k=0}^{\infty} \{\hat{v}_k^{(3)} \exp(\zeta_k z_\tau) + \hat{w}_k^{(3)} \exp(\zeta_k(\tau h - z_\tau))\} \\
 g_2(\bar{z}_\tau) &= \overline{g_1(z_\tau)}
 \end{aligned}
 \tag{20}$$

where

$$\xi_m = \begin{cases} -\frac{m_0\pi i}{\tau h} & \text{if } m = 0 \\ -\frac{m\pi i}{\tau h} & \text{if } m \geq 1 \end{cases} \quad \zeta_k = \begin{cases} \frac{k_0\pi i}{L_1} & \text{if } k = 0 \\ \frac{k\pi i}{L_1} & \text{if } k \geq 1 \end{cases}
 \tag{21}$$

The functions  $\exp(\eta_{m\alpha} z_\alpha)$  in Eq. (18) vary sinusoidally on the surface  $x_1 = 0$  of the  $n$ th lamina and decay exponentially in the  $x_1$ -direction. With increasing  $m$ , higher harmonics are introduced on the surface  $x_1 = 0$  accompanied by steeper exponential decay in the  $x_1$ -direction. Similarly, functions  $\exp(\eta_{m\alpha}(l - z_\alpha)), \exp(\lambda_{k\alpha} z_\alpha)$ , and  $\exp(\lambda_{k\alpha}(p_\alpha h - z_\alpha))$  vary sinusoidally on surfaces  $x_1 = L_1, x_3 = 0$ , and  $x_3 = h$ , respectively. The inequality (12)<sub>1</sub> ensures that all functions decay exponentially toward the interior of the lamina. Equations (18)<sub>2</sub> and (20)<sub>2</sub> for  $f_{\alpha+4}(\bar{z}_\alpha)$  and  $g_2(\bar{z}_\tau)$  ensure

that mechanical displacements, stresses, the electric potential, the electric displacement, the temperature change, and the heat flux are real valued.

The unknown coefficients  $v_{k\alpha}^{(s)}, w_{k\alpha}^{(s)}, \hat{v}_k^{(s)}, \hat{w}_k^{(s)}$  ( $s = 1, 3$ ) in the series are assumed to be complex for  $k \neq 0$  and real when  $k = 0$ . The superscript  $s = 1, 3$  indicates that the exponential function associated with the unknown has a sinusoidal variation on the surface  $x_s = \text{const}$ . Substituting Eqs. (18) and (20) into Eq. (13) results in the following expression for the mechanical displacement, the electric potential, and the temperature change for nondegenerate materials

$$\begin{aligned} \begin{bmatrix} \mathbf{u} \\ \phi \end{bmatrix} &= \mathbf{A} \left\{ \sum_{m=0}^{\infty} [\langle \exp(\eta_{m*} z_*) \rangle \mathbf{v}_m^{(1)} + \langle \exp(\eta_{m*} (l - z_*)) \rangle \mathbf{w}_m^{(1)}] \right. \\ &\quad \left. + \sum_{k=0}^{\infty} [\langle \exp(\lambda_{k*} z_*) \rangle \mathbf{v}_k^{(3)} + \langle \exp(\lambda_{k*} (p_* h - z_*)) \rangle \mathbf{w}_k^{(3)}] \right\} \\ &+ \mathbf{c} \left\{ \sum_{m=0}^{\infty} [\exp(\xi_m z_\tau) \hat{v}_m^{(1)} + \exp(\xi_m (l - z_\tau)) \hat{w}_m^{(1)}] \right. \\ &\quad \left. + \sum_{k=0}^{\infty} [\exp(\zeta_k z_\tau) \hat{v}_k^{(3)} + \exp(\zeta_k (\tau h - z_\tau)) \hat{w}_k^{(3)}] \right\} + \text{conjugate} \quad (22) \\ T &= \left\{ \sum_{m=0}^{\infty} [\xi_m \exp(\xi_m z_\tau) \hat{v}_m^{(1)} - \xi_m \exp(\xi_m (l - z_\tau)) \hat{w}_m^{(1)}] \right. \\ &\quad \left. + \sum_{k=0}^{\infty} [\zeta_k \exp(\zeta_k z_\tau) \hat{v}_k^{(3)} - \zeta_k \exp(\zeta_k (\tau h - z_\tau)) \hat{w}_k^{(3)}] \right\} + \text{conjugate} \end{aligned}$$

where

$$\begin{aligned} \mathbf{A} &= [\mathbf{a}_1, \mathbf{a}_2, \mathbf{a}_3, \mathbf{a}_4] \quad \langle \psi(z_*) \rangle = \text{diag}[\psi(z_1), \psi(z_2), \psi(z_3), \psi(z_4)] \\ (\mathbf{v}_m^{(s)})_\alpha &= v_{m\alpha}^{(s)} \quad (\mathbf{w}_m^{(s)})_\alpha = w_{m\alpha}^{(s)} \quad \alpha = 1, \dots, 4 \end{aligned}$$

and conjugate stands for the complex conjugate of the explicitly stated terms. Expressions for stress components and the electric displacement vector, obtained by substituting Eqs. (18) and (20) into Eqs. (14)<sub>1,2</sub> are

$$\begin{aligned} \begin{bmatrix} \boldsymbol{\sigma}_1 \\ D_1 \end{bmatrix} &= \mathbf{B} \left\{ \sum_{m=0}^{\infty} [-\langle p_* \eta_{m*} \exp(\eta_{m*} z_*) \rangle \mathbf{v}_m^{(1)} + \langle p_* \eta_{m*} \exp(\eta_{m*} (l - z_*)) \rangle \mathbf{w}_m^{(1)}] \right. \\ &\quad \left. + \sum_{k=0}^{\infty} [-\langle p_* \lambda_{k*} \exp(\lambda_{k*} z_*) \rangle \mathbf{v}_k^{(3)} + \langle p_* \lambda_{k*} \exp(\lambda_{k*} (p_* h - z_*)) \rangle \mathbf{w}_k^{(3)}] \right\} \\ &+ \boldsymbol{\tau} \mathbf{d} \left\{ \sum_{m=0}^{\infty} [-\xi_m \exp(\xi_m z_\tau) \hat{v}_m^{(1)} + \xi_m \exp(\xi_m (l - z_\tau)) \hat{w}_m^{(1)}] \right. \\ &\quad \left. + \sum_{k=0}^{\infty} [-\zeta_k \exp(\zeta_k z_\tau) \hat{v}_k^{(3)} + \zeta_k \exp(\zeta_k (\tau h - z_\tau)) \hat{w}_k^{(3)}] \right\} + \text{conjugate} \quad (23) \end{aligned}$$

$$\begin{aligned}
 \begin{bmatrix} \boldsymbol{\sigma}_3 \\ D_3 \end{bmatrix} &= \mathbf{B} \left\{ \sum_{m=0}^{\infty} [\langle \eta_{m*} \exp(\eta_{m*} z_*) \rangle \mathbf{v}_m^{(1)} - \langle \eta_{m*} \exp(\eta_{m*} (l - z_*)) \rangle \mathbf{w}_m^{(1)}] \right. \\
 &\quad \left. + \sum_{k=0}^{\infty} [\langle \lambda_{k*} \exp(\lambda_{k*} z_*) \rangle \mathbf{v}_k^{(3)} - \langle \lambda_{k*} \exp(\lambda_{k*} (p_* h - z_*)) \rangle \mathbf{w}_k^{(3)}] \right\} \\
 &+ \mathbf{d} \left\{ \sum_{m=0}^{\infty} [\zeta_m \exp(\zeta_m z_\tau) \hat{\mathbf{v}}_m^{(1)} - \zeta_m \exp(\zeta_m (l - z_\tau)) \hat{\mathbf{w}}_m^{(1)}] \right. \\
 &\quad \left. + \sum_{k=0}^{\infty} [\zeta_k \exp(\zeta_k z_\tau) \hat{\mathbf{v}}_k^{(3)} - \zeta_k \exp(\zeta_k (\tau h - z_\tau)) \hat{\mathbf{w}}_k^{(3)}] \right\} + \text{conjugate} \quad (24)
 \end{aligned}$$

where  $\mathbf{B} = [\mathbf{b}_1, \mathbf{b}_2, \mathbf{b}_3, \mathbf{b}_4]$ . The expression for the heat flux obtained by substituting Eqs. (18) and (20) into Eq. (14)<sub>3</sub> is

$$\begin{aligned}
 \mathbf{q} &= -(\kappa_1 + \tau \kappa_3) \left\{ \sum_{m=0}^{\infty} [\zeta_m^2 \exp(\zeta_m z_\tau) \hat{\mathbf{v}}_m^{(1)} + \zeta_m^2 \exp(\zeta_m (l - z_\tau)) \hat{\mathbf{w}}_m^{(1)}] \right. \\
 &\quad \left. + \sum_{k=0}^{\infty} [\zeta_k^2 \exp(\zeta_k z_\tau) \hat{\mathbf{v}}_k^{(3)} + \zeta_k^2 \exp(\zeta_k (\tau h - z_\tau)) \hat{\mathbf{w}}_k^{(3)}] \right\} + \text{conjugate} \quad (25)
 \end{aligned}$$

### SATISFACTION OF BOUNDARY AND INTERFACE CONDITIONS

Each lamina has a set of coefficients  $\mathbf{v}_k^{(s)}, \mathbf{w}_k^{(s)}, \hat{\mathbf{v}}_k^{(s)}, \hat{\mathbf{w}}_k^{(s)}$  ( $s = 1, 3$ ) that are determined by the classical Fourier series method from the interface continuity conditions and boundary conditions on all surfaces of the laminate.

Since the heat conduction problem is uncoupled from the mechanical problem, we first determine the temperature field by imposing the thermal boundary conditions on the four bounding surfaces of the laminate and the continuity of temperature and the heat flux across interfaces between adjoining laminae. On the top surface  $x_3 = L_3^{(N+1)}$  of the laminate, we extend the component functions defined over  $(0, L_1)$  in Eq. (22)<sub>2</sub> to the interval  $(-L_1, 0)$  in the  $x_1$ -direction. The functions  $\exp(\zeta_k z_\tau)$  and  $\exp(\zeta_k (\tau h - z_\tau))$  that are sinusoidal in the  $x_1$ -direction are extended without modification since they form the basis functions on this surface, except for  $\exp(\zeta_0 z_\tau)$  and  $\exp(\zeta_0 (\tau h - z_\tau))$  that are extended as even functions since they represent the constant terms in the Fourier series representation. The functions  $\exp(\zeta_m z_\tau)$  and  $\exp(\zeta_m (l - z_\tau))$  are extended as even functions since they vary exponentially in the  $x_1$ -direction. We multiply Eq. (6)<sub>2</sub> for  $s = 3$  by  $\exp(j\pi i x_1 / L_1)$  and integrate the result with respect to  $x_1$  from  $-L_1$  to  $L_1$  to obtain

$$\int_{-L_1}^{L_1} \{ \tilde{\mathbf{m}}^{(3)} T + \tilde{\mathbf{r}}^{(3)} q_3 - \tilde{\varphi}^{(3)} \} \exp(j\pi i x_1 / L_1) dx_1 = 0 \quad (x_3 = L_3^{(N+1)}; j = 1, 2, 3, \dots) \quad (26)$$

The same procedure is used to enforce the thermal boundary conditions (6) for the bottom surface, the edges, and the interface thermal continuity conditions (7)<sub>5,6</sub>. Substituting for  $T$  and  $\mathbf{q}$  into Eq. (26) and the other equations that enforce the thermal boundary and interface continuity conditions results in a nonstandard infinite set of linear equations for the unknowns  $\hat{v}_k^{(s)}, \hat{\mathbf{w}}_k^{(s)}$  ( $s = 1, 3$ ).

The electromechanical boundary conditions (5) and interface continuity conditions (7) or (8) for the displacements and tractions are also enforced in a similar manner. For example, the mechanical boundary conditions on the surface  $x_3 = L_3^{(N+1)}$  will give

$$\int_{-L_1}^{L_1} \left\{ \mathbf{J}_{u\phi}^{(3)} \begin{bmatrix} \mathbf{u} \\ \phi \end{bmatrix} + \mathbf{J}_{\sigma D}^{(3)} \begin{bmatrix} \boldsymbol{\sigma}_3 \\ D_3 \end{bmatrix} - \mathbf{g}^{(3)} \right\} \exp(j\pi i x_1 / L_1) dx_1 = 0$$

$$(x_3 = L_3^{(N+1)}; j = 1, 2, 3, \dots) \tag{27}$$

Enforcing all electromechanical boundary and interface conditions will yield another nonstandard infinite set of linear equations for  $\mathbf{v}_m^{(s)}$  and  $\mathbf{w}_m^{(s)}$ . A general theory for the resulting infinite system of equations does not exist. However, reasonably accurate solutions may be obtained by truncating the series involving summations over  $m$  and  $k$  in Eqs. (18) and (20) to  $M^{(n)}$  and  $K$  terms, respectively. In general, we try to maintain approximately the same period of the largest harmonic on all interfaces and boundaries by choosing  $M^{(n)} = \text{Ceil}(Kh^{(n)}/L_1)$ , where  $\text{Ceil}(y)$  gives the smallest integer greater than or equal to  $y$ . The truncated set of coefficients  $\hat{v}_k^{(s)}, \hat{\mathbf{w}}_k^{(s)}$  are determined first by solving the truncated set of linear equations corresponding to the heat conduction problem. The truncated set of coefficients  $\mathbf{v}_m^{(s)}, \mathbf{w}_m^{(s)}$  are determined next by solving the truncated system of linear equations obtained by enforcing the mechanical boundary and interface continuity conditions.

The solution (22) indicates that the component functions decrease exponentially from the boundary/interfaces into the interior of the  $n$ th lamina. By truncating the series, we have effectively ignored coefficients with suffices greater than a particular value and approximated coefficients of the remaining terms in the series. Due to the rapid decay of component functions associated with large suffices, the truncation of the series will not greatly influence the solution at the interior points. A larger value of  $K$  is expected to give a more accurate solution at points close to the boundary and interfaces. Note that the coefficients  $\mathbf{v}_k^{(3)}$  and  $\mathbf{w}_k^{(3)}$  in the expressions for the stresses and electric displacements in Eqs. (23) and (24) are multiplied by  $\lambda_{k*}$ , and  $\mathbf{v}_m^{(1)}$  and  $\mathbf{w}_m^{(1)}$  are multiplied by  $\eta_{m*}$ . However, the coefficients of these terms in the expressions (22)<sub>1</sub> for displacements are unity. Since  $\lambda_{k*}$  and  $\eta_{m*}$  increase as the suffices  $k$  and  $m$  increase, the terms with large suffices are more significant for the stresses than for the displacements. Thus, the stresses will converge more slowly than the displacements. After coefficients have been determined by satisfying the boundary and the interface conditions, displacements, the electric potential, stresses, the electric displacement, the temperature, and the heat flux at any point can be obtained from Eqs. (22)–(25).

## RESULTS AND DISCUSSION

We present results for hybrid laminates with each lamina made of either graphite/epoxy (Gr/Ep) or PZT-5A. The principal material axis of the Gr/Ep lamina is assumed to be in the  $x_1$ - $x_2$  plane and inclined at an angle  $\psi$  to the  $x_1$ -axis. The nonzero values of material properties for the Gr/Ep are listed in Table 1 for  $\psi = 0^\circ$ ,  $90^\circ$ , and  $\pm 45^\circ$ . We consider two types of piezoelectric actuators, namely thickness poled PZT-5A and axially poled PZT-5A. Thickness poled piezoelectric materials are poled in the  $x_3$ -direction and their primary mode of actuation is by extension/contraction in the  $x_1$ - $x_2$  plane when subjected to an electric field in the thickness direction. Thickness poled piezoelectric materials are the most common type used as sensors and actuators. Axially poled piezoelectric materials are poled in the  $x_1$ -direction, and their primary mode of actuation is by transverse shear strain in the  $x_1$ - $x_3$  plane when it is subjected to an electric field in the thickness direction. This is the lesser known shear mode that has been studied by Borieseiko et al. [37], Zhang and Sun [38], Benjeddou et al. [39], Vel and Batra [40, 41], and Batra and Geng [42]. Different piezoceramic constants are effective in the extension and shear mode piezoceramic plates; their nonzero material parameters are given in Table 1. The material properties of the axially poled PZT-5A were obtained by a tensor transformation of the material properties given by Xu et al. [19] for thickness poled PZT-5A. In this section, we denote the thickness of the plate by  $H$ , its length by  $L$ , and the length-to-thickness ratio  $L/H$  by  $S$ .

### Validation of the Approach

The solution procedure is validated by comparing our results with the exact results given by Dube et al. [15] for a simply supported cadmium selenide plate that is exposed to an ambient temperature on the top surface through a boundary conductance. The geometry, material properties, applied loads, and normalization of the results are the same as those employed by Dube et al. [15]. Values computed using  $K = 500$  terms are given in Table 2 for a thick plate with length-to-thickness ratio  $S = 2$  and for a thin plate with  $S = 20$ . Results for displacements, stresses, the electric potential, the electric displacements, and the temperature change are essentially identical to those obtained by Dube et al. [15].

### Thickness Poled Piezoelectric Materials

We analyze plates made of either homogeneous thickness poled PZT-5A or laminated plates consisting of Gr/Ep and PZT-5A laminae. The edges  $x_1 = 0$  and  $L$  are either clamped ( $u_1 = u_2 = u_3 = 0$ ) or traction-free ( $\sigma_{11} = \sigma_{12} = \sigma_{13} = 0$ ) or simply supported ( $\sigma_{11} = \sigma_{12} = 0$ ,  $u_3 = 0$ ). For laminates with thickness poled piezoelectric materials we study the effect of thermal loads only since a three-dimensional solution for mechanical and electrical loads has already been given by Vel and Batra [29]. For the linear problem considered here, results for combined mechanical, electrical, and thermal loads can be obtained by the superposition of results for each of the three loads.

**Table 1 Material properties of the graphite-epoxy and PZT-5A layers**

Material Property	Gr/Ep 0°	Gr/Ep 90°	Gr/Ep ±45°	Thickness Poled PZT-5A	Axially Poled PZT-5A
$C_{1111}$ (GPa)	183.44	11.662	58.128	99.201	86.856
$C_{2222}$ (GPa)	11.662	183.44	58.128	99.201	99.201
$C_{3333}$ (GPa)	11.662	11.662	11.662	86.856	99.201
$C_{1122}$ (GPa)	4.363	4.363	43.788	54.016	50.778
$C_{1133}$ (GPa)	4.363	3.918	4.140	50.778	50.778
$C_{2233}$ (GPa)	3.918	4.363	4.140	50.778	54.016
$C_{2323}$ (GPa)	2.870	7.170	5.020	21.100	22.593
$C_{3131}$ (GPa)	7.170	2.870	5.020	21.100	21.100
$C_{1212}$ (GPa)	7.170	7.170	46.595	22.593	21.100
$C_{1112}$ (GPa)	0	0	±42.945	0	0
$C_{2212}$ (GPa)	0	0	±42.945	0	0
$C_{3312}$ (GPa)	0	0	±0.2222	0	0
$C_{2331}$ (GPa)	0	0	±2.150	0	0
$\beta_{11}$ ( $10^5$ Pa K <sup>-1</sup> )	2.000	3.506	7.580	3.314	3.260
$\beta_{22}$ ( $10^5$ Pa K <sup>-1</sup> )	3.506	2.000	7.280	3.314	3.314
$\beta_{12}$ ( $10^5$ Pa K <sup>-1</sup> )	0	0	±4.484	0	0
$\beta_{33}$ ( $10^5$ Pa K <sup>-1</sup> )	3.506	3.506	3.531	3.260	3.314
$e_{111}$ (C m <sup>-2</sup> )	0	0	0	0	15.118
$e_{122}$ (C m <sup>-2</sup> )	0	0	0	0	-7.209
$e_{133}$ (C m <sup>-2</sup> )	0	0	0	0	-7.209
$e_{113}$ (C m <sup>-2</sup> )	0	0	0	12.322	0
$e_{223}$ (C m <sup>-2</sup> )	0	0	0	12.322	0
$e_{212}$ (C m <sup>-2</sup> )	0	0	0	0	12.322
$e_{311}$ (C m <sup>-2</sup> )	0	0	0	-7.209	0
$e_{322}$ (C m <sup>-2</sup> )	0	0	0	-7.209	0
$e_{333}$ (C m <sup>-2</sup> )	0	0	0	15.118	0
$e_{313}$ (C m <sup>-2</sup> )	0	0	0	0	12.322
$\epsilon_{11}$ ( $10^{-10}$ F/m)	153.0	153.0	153.0	153.0	150.0
$\epsilon_{22}$ ( $10^{-10}$ F/m)	153.0	153.0	153.0	153.0	153.0
$\epsilon_{33}$ ( $10^{-10}$ F/m)	153.0	153.0	153.0	150.0	153.0
$r_1$ (Cm <sup>-2</sup> K <sup>-1</sup> )	0	0	0	0	0.0007
$r_3$ (Cm <sup>-2</sup> K <sup>-1</sup> )	0	0	0	0.0007	0
$\kappa_{11}$ (Wm <sup>-1</sup> K <sup>-1</sup> )	1.5	0.5	1.0	1.8	1.8
$\kappa_{22}$ (Wm <sup>-1</sup> K <sup>-1</sup> )	0.5	1.5	1.0	1.8	1.8
$\kappa_{12}$ (Wm <sup>-1</sup> K <sup>-1</sup> )	0	0	±0.5	0	0
$\kappa_{33}$ (Wm <sup>-1</sup> K <sup>-1</sup> )	0.5	0.5	0.5	1.8	1.8

The top and bottom surfaces of the piezoelectric layer are electroded; the bottom surface is maintained at the reference temperature and free of traction, that is,  $T(x_1, 0) = 0$ , and  $\sigma_3(x_1, 0) = \sigma_3(x_1, H) = 0$ . The top surface  $x_3 = H$  is subjected to the sinusoidal temperature change

$$T(x_1, H) = T_0 \sin \frac{\pi x_1}{L} \tag{28}$$

The edges  $x_1 = 0, L$  are electrically grounded ( $\phi = 0$ ) and maintained at the reference temperature ( $T = 0$ ). The mechanical displacements, stresses, electric displacements, the electric potential, and the temperature change are nondimensionalized as

**Table 2 Comparison of the present solution for a single-layer cadmium selenide plate with the exact results of Dube et al. [15]**

Normalized Results	S = 2		S = 20	
	Dube et al. [15]	Present Analysis	Dube et al. [15]	Present Analysis
$10^2 \bar{u}_1(0, H)$	-29.33	-29.330	-43.11	-43.112
$10^2 \bar{u}_3(\frac{L}{2}, \frac{H}{2})/S$	4.832	4.8325	2.313	2.3126
$10^2 \bar{\sigma}_{11}(\frac{L}{2}, H)S^2$	-6.236	-6.2361	-14.37	-14.374
$10^2 \bar{\sigma}_{13}(0, \frac{H}{4})S^3$	1.660	1.6597	4.226	4.2262
$10^2 \bar{\sigma}_{33}(\frac{L}{2}, \frac{H}{2})S^4$	1.759	1.7586	4.426	4.4265
$10^4 \bar{\phi}(\frac{L}{2}, \frac{H}{2})S$	8.946	8.9457	5.195	5.1949
$\bar{T}(\frac{L}{2}, H)$	0.6357	0.63570	0.9172	0.91724
$\bar{D}_3(\frac{L}{2}, H)$	-1.622	-1.6220	-3.125	-3.1254

$$\begin{aligned}
 \bar{u}_i &= \frac{u_i}{L\alpha_0 T_0} & \bar{\sigma}_{ij} &= \frac{\sigma_{ij}}{C_0\alpha_0 T_0} & \bar{\phi} &= \frac{e_0\phi}{C_0L\alpha_0 T_0} \\
 \bar{D}_i &= \frac{D_i}{e_0\alpha_0 T_0} & \bar{T} &= \frac{T}{T_0}
 \end{aligned}
 \tag{29}$$

where  $C_0 = 99.201$  GPa,  $e_0 = 7.209$  C·m<sup>-2</sup>, and  $\alpha_0 = 1.5 \times 10^{-6}$  K<sup>-1</sup> are representative moduli of PZT-5A.

**Homogeneous plates.** The first example concerns a homogeneous PZT-5A plate poled in the thickness direction. The plate is clamped at  $x_1 = 0$  and simply supported at  $x_1 = L$ . The top and bottom surfaces are electrically grounded. The effect of truncation of series on the solution is investigated for a thick clamped simply supported laminate. Table 3 shows that the values of the normalized mechanical displacements, stresses, the electric potential, the electric displacement, and the temperature have converged to at least four significant digits with  $K = 500$  terms, while reasonable accuracy may be obtained with 100 terms. Although  $k_0$  in Eqs. (19) and (21) was chosen to be 0.5 for this study, a similar convergence behavior was observed for other values of  $k_0$ . All results in the tables and plots to follow are obtained by retaining 500 terms in the series solution.

The longitudinal variation of the transverse deflection, the electric potential, the transverse shear stress, and the transverse normal stress is shown in Figure 2 for three different length-to-thickness ratios of the clamped simply supported plate subjected to the thermal load. Steep gradients in the transverse shear and normal stresses at  $x_1 = 0$ , shown in Figures 2(c, d), are due to the well-known boundary layer effects at the clamped edge, which is absent at the simply supported edge. It is observed that the axial width of the boundary layer region is inversely proportional to the aspect ratio  $S$  of the plate. Figure 3 shows on four cross-sections, the through-the-thickness variation of the axial displacement, longitudinal stress, transverse shear stress, and transverse normal stress for  $S = 4$ . The axial displacement  $\bar{u}_1$  has an almost linear variation in the thickness direction, except within the boundary layer.

**Table 3 Convergence study for a homogeneous thickness poled PZT-5A clamped simply supported plate subjected to the thermal load,  $S = 5$**

$K$	$\bar{u}_3(\frac{L}{2}, \frac{H}{2})$	$\bar{\sigma}_{11}(\frac{L}{2}, H)$	$10\bar{\sigma}_{13}(\frac{L}{4}, \frac{H}{2})$	$10^4\bar{\sigma}_{33}(\frac{L}{2}, \frac{H}{2})$	$10^2\bar{\phi}(\frac{L}{2}, \frac{H}{2})$	$\bar{D}_3(\frac{L}{2}, H)$	$\bar{T}(\frac{L}{2}, \frac{H}{2})$
50	1.5147	-1.2555	1.4351	18.887	-5.3005	33.564	0.46378
100	1.5125	-1.2519	1.4371	18.889	-5.3013	33.592	0.46378
200	1.5116	-1.2534	1.4380	18.891	-5.3016	33.588	0.46378
300	1.5114	-1.2538	1.4382	18.891	-5.3017	33.587	0.46378
400	1.5113	-1.2540	1.4383	18.891	-5.3017	33.586	0.46378
500	1.5112	-1.2541	1.4384	18.891	-5.3018	33.586	0.46378

The transverse shear stress  $\bar{\sigma}_{13}$  takes on the classic parabolic distribution at the midspan location and near the simply supported edge. However, within the boundary layer region at  $x_1/L = 0.01$ , the transverse shear stress  $\bar{\sigma}_{13}$  has steep gradients at the top and bottom surfaces; the maximum value occurs at  $x_3 \simeq 0.05H$  and  $0.95H$ , while the minimum transverse shear stress occurs at the midsurface. The magnitude of the transverse normal stress  $\bar{\sigma}_{33}$  within the boundary layer region

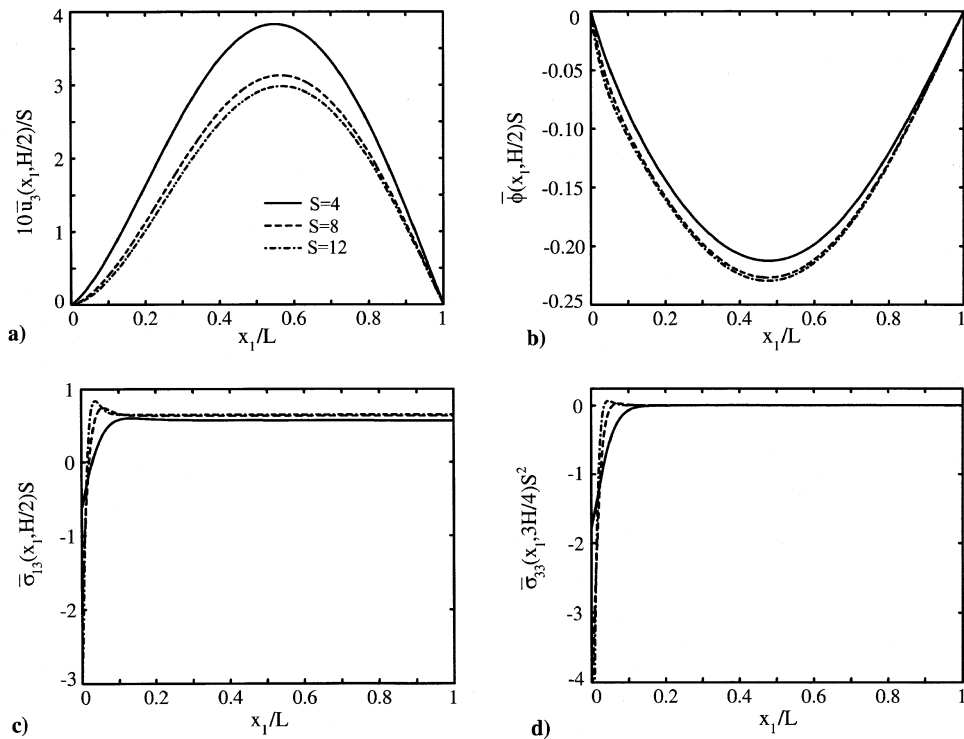


**Figure 2.** Longitudinal variation of (a) transverse displacement, (b) electric potential, (c) transverse shear stress, and (d) transverse normal stress for a homogeneous thickness poled PZT-5A clamped simply supported plate for the thermal load and length-to-thickness ratios  $S = 4, 8,$  and  $12$ .

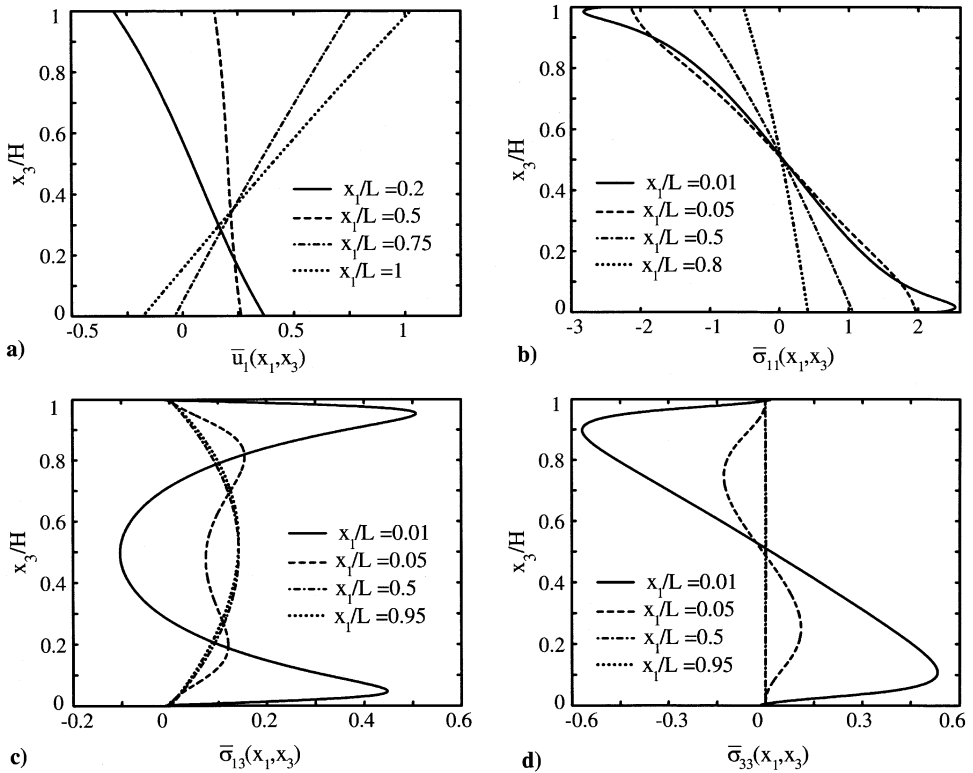


**Figure 3.** Through-the-thickness distribution of (a) axial deflection, (b) longitudinal stress, (c) transverse shear stress, and (d) transverse normal stress for a homogeneous thickness poled PZT-5A clamped simply supported plate for the thermal load and length-to-thickness ratio  $S = 4$ .

is significantly larger than that at any other region of the plate. The transverse normal stress at  $x_1/L = 0.01$  also has steep gradients at the top and bottom surfaces; its magnitude is largest at  $x_3 \simeq 0.1H$  and  $0.9H$  and equals nearly 30% of the magnitude of the longitudinal stress there.

Results for a clamped-free homogeneous PZT-5A plate poled in the thickness direction and subjected to the thermal load are presented in Figure 4. The longitudinal variation of the transverse shear and normal stresses on three horizontal planes is depicted in Figures 4(a, b). It is observed that the transverse normal stress is largest at the clamped edge. Sharp gradients near the clamped and free edges in the distribution of the normal stress are indicative of the boundary layer effects near these edges. The electric potential has a parabolic profile in the thickness direction as shown in Figure 4(c). It suggests that a plate theory should have at least quadratic terms in the expansion for the electric potential in the thickness direction. Through-the-thickness variations of the transverse shear stress at  $x_1/L = 0.05, 0.1, 0.3,$  and  $0.9$  are given in Figure 4(d). Numerical results at specific locations for clamped simply supported plates for length-to-thickness ratios  $S = 4, 8,$  and  $12$  are given in Table 4.

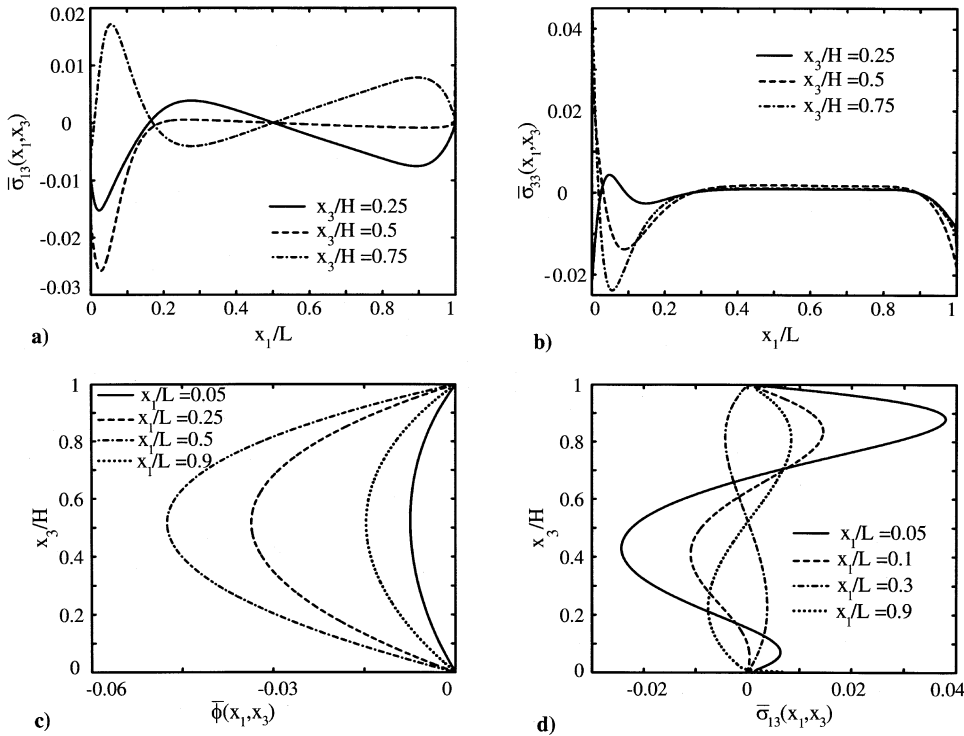


**Figure 4.** Longitudinal variation of (a) transverse shear stress, (b) transverse normal stress, and through-the-thickness variation of (c) electric potential, and (d) transverse shear stress for a homogeneous thickness poled PZT-5A cantilever plate for the thermal load and length-to-thickness ratio  $S = 4$ .

**Table 4** Displacements, stresses, electric potential, electric displacement, and temperature change for homogeneous thickness poled PZT-5A clamped simply supported plates for the thermal load and length-to-thickness ratios  $S = 4, 8, \text{ and } 12$

Variable	$S = 4$	$S = 8$	$S = 12$
$10\bar{u}_1(3L/4, H)$	7.5473	7.0583	6.9431
$10\bar{u}_3(L/2, H/2)/S$	3.7780	3.0513	2.8940
$\bar{\sigma}_{11}(L/2, H)$	-1.2541	-1.2980	-1.3107
$\bar{\sigma}_{11}(L/2, 0)$	1.0590	1.2461	1.2874
$\bar{\sigma}_{13}(L/2, H/2)S$	0.5695	0.6339	0.6487
$\bar{\sigma}_{13}(L/12, H/2)S$	0.5339	0.6932	0.6618
$\bar{\sigma}_{33}(L/12, 3H/4)S^2$	-0.5806	0.1820	0.0742
$10\bar{\phi}(L/4, H/2)S$	-1.6556	-1.7943	-1.8200
$\bar{D}_1(L/4, H/2)S/10$	2.1919	2.2310	2.2484
$\bar{D}_3(L/2, H)/10$	3.3586	3.3513	3.3500
$\bar{T}(L/2, H/2)$	0.4638	0.4905	0.4957

**Hybrid laminated plates.** A multilayered cross-ply plate consisting of three layers in which the bottom two layers are made of Gr/Ep and the top layer is made of thickness poled PZT-5A is studied next. The fibers are oriented parallel and perpendicular to the  $x_1$ -axis in the bottom and middle layers, respectively, that is, it is a  $[0^\circ \text{ Gr/Ep}, 90^\circ \text{ Gr/Ep}, \text{ extension PZT-5A}]$  laminate. The Gr/Ep laminae are of thicknesses  $0.4H$ , and the PZT-5A lamina is of thickness  $0.2H$ . The top and bottom surfaces of the PZT-5A lamina are electroded and electrically grounded, and the laminae are assumed to be perfectly bonded to each other. As in the case of the homogeneous piezoelectric plate studied earlier, the top and bottom surfaces are free of external traction. Through-the-thickness variations of the axial and transverse displacements, electric potential, and transverse shear stresses for a clamped simply supported multilayer plate with  $S = 4$  are presented in Figure 5 for the thermal load applied to the top surface. As is evident from Figures 5(a, b), the continuity of the displacements at the interfaces  $x_3/H = 0.4$  and  $0.8$  between adjoining laminae are satisfied very well. The transverse elongation, which is the difference between the transverse displacements of the corresponding points on the top and bottom surfaces shown in Figure 5(b), is significant due to the thermal load. Since our analysis is

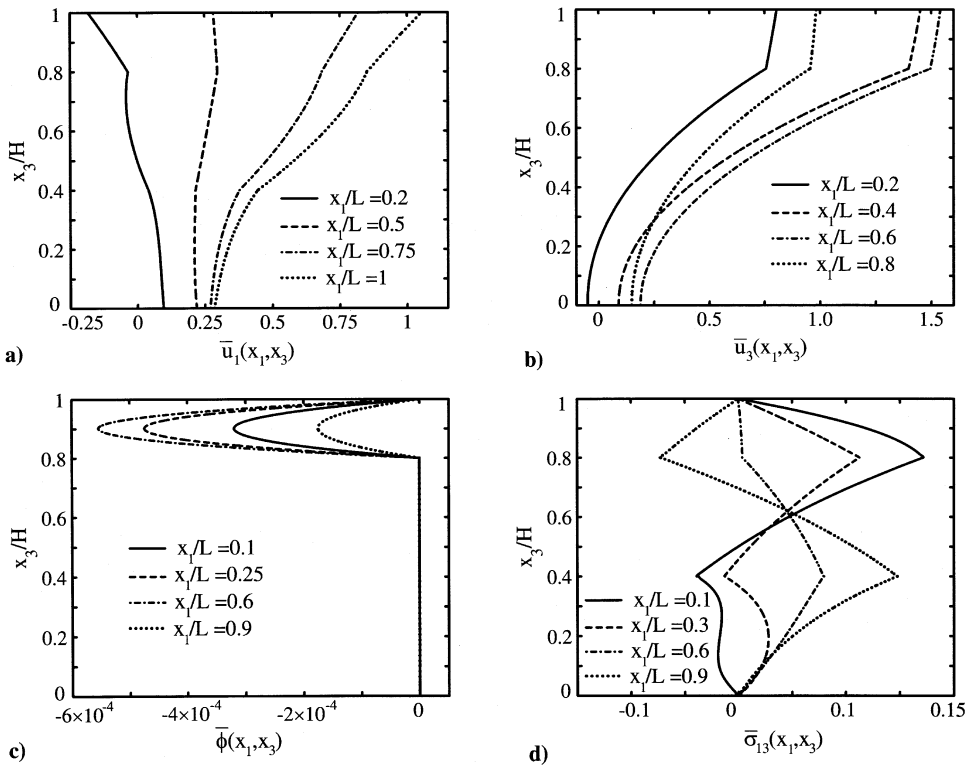


**Figure 5.** Through-the-thickness distribution of (a) axial deflection, (b) transverse deflection, (c) electric potential, and (d) transverse shear stress for a laminated  $[0^\circ \text{ Gr/Ep}, 90^\circ \text{ Gr/Ep}, \text{ thickness poled PZT-5A}]$  clamped simply supported plate for the thermal load and length-to-thickness ratio  $S = 4$ .

based on three-dimensional thermopiezoelectricity, it is able to capture the thickness distention of the laminate, unlike many plate theories that neglect this effect. The total electric potential, which is the sum of the electric potential due to the thermal deformation and the pyroelectric effect has a parabolic through-the-thickness profile in the PZT. The transverse shear stress, depicted in Figure 5(d), is seen to be largest either at the interface between the Gr/Ep laminae or the interface between the Gr/Ep and the PZT.

Next, consider an angle-ply multilayered laminate that also consists of three layers with the bottom and middle layers made of Gr/Ep and a PZT-5A top layer, except that the fibers are oriented at  $45^\circ$  and  $-45^\circ$  to the  $x_1$ -axis in the bottom and middle layers, respectively, to form a  $[45^\circ \text{ Gr/Ep}, -45^\circ \text{ Gr/Ep}, \text{extension PZT-5A}]$  laminate. The boundary conditions are identical to the cross-ply laminate studied earlier. Through-the-thickness profiles of the displacement and stress components are given in Figure 6 for the thermal load. As expected, the nondimensionalized longitudinal stress  $\bar{\sigma}_{11}$  is discontinuous at the interfaces between the laminae due to the abrupt change in material properties. However, the transverse shear stresses  $\bar{\sigma}_{13}$  and  $\bar{\sigma}_{23}$ , shown in Figures 6(c, d), are continuous at points on the interfaces.

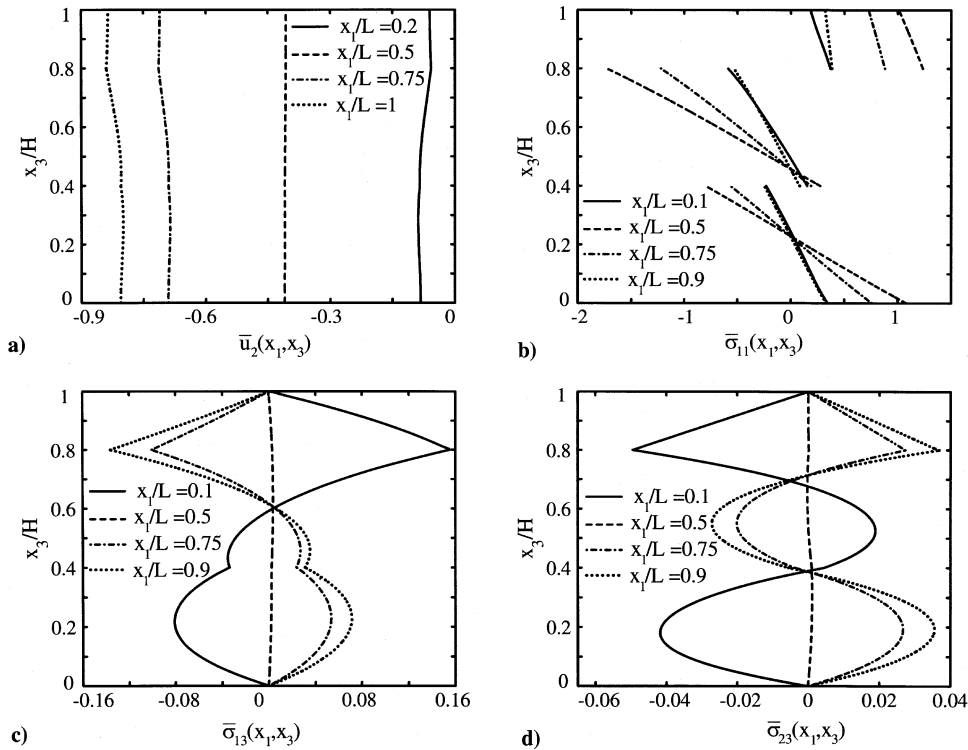


**Figure 6.** Through-the-thickness distribution of (a) axial deflection, (b) transverse deflection, (c) electric potential, and (d) transverse shear stress for a laminated  $[45^\circ \text{ Gr/Ep}, -45^\circ \text{ Gr/Ep}, \text{thickness poled PZT-5A}]$  clamped simply supported plate for the thermal load and length-to-thickness ratio  $S = 4$ .

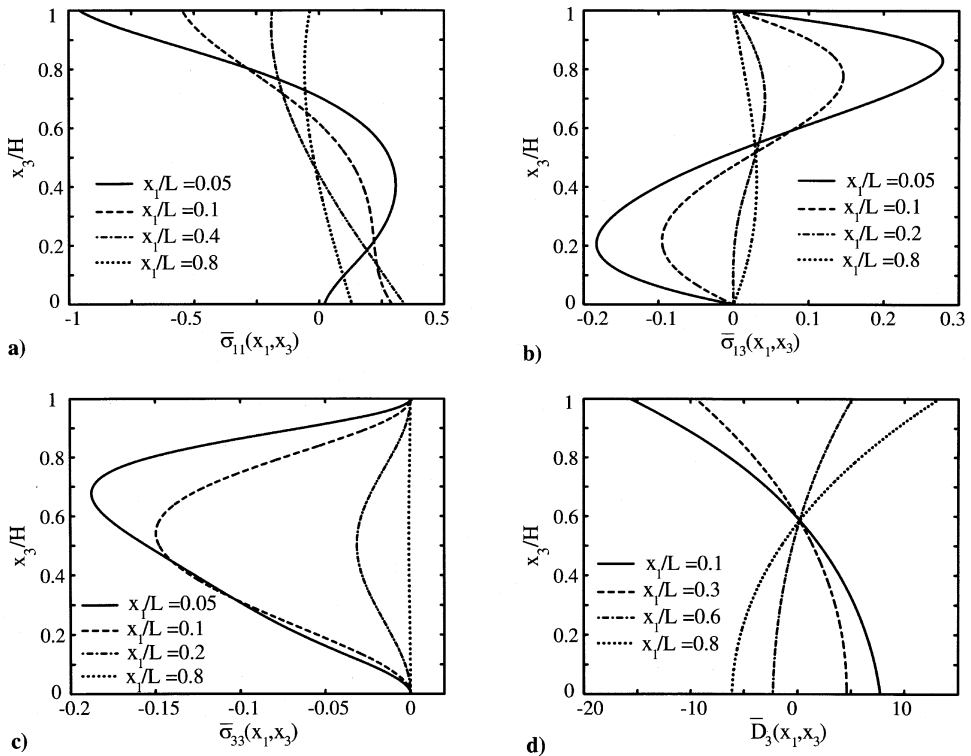
**Axially Poled Piezoelectric Materials**

**Homogeneous plates.** Consider a clamped simply supported homogeneous shear mode PZT-5A plate that is poled in the  $x_1$ -direction. The top and bottom surfaces are electroded. The bottom surface is maintained at the reference temperature and is traction free, that is,  $T(x_1, 0) = 0$  and  $\sigma_3(x_1, 0) = \mathbf{0}$ . The edges of the plate are free of electric charge, that is,  $D_1 = 0$  at  $x_1 = 0, L$ . In addition to the thermal load (28), we also consider the electrical load

$$[\phi(x_1, 0), \phi(x_1, H)] = \frac{1}{2}[-\phi_0, \phi_0] \cos \frac{\pi x_1}{L} \quad T(x_1, H) = 0 \quad \sigma_3(x_1, H) = \mathbf{0} \quad (30)$$

The mechanical displacements, stresses, electric displacements, electric potential, and temperature change are nondimensionalized as

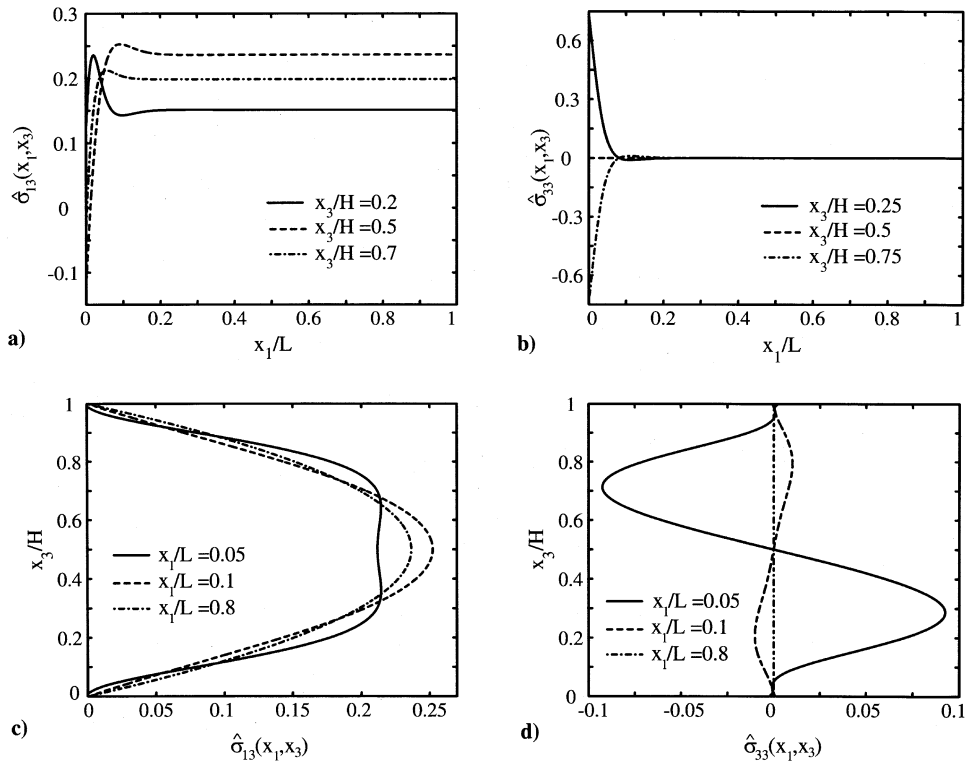
$$\hat{u}_i = \frac{u_i C_0}{e_0 \phi_0} \quad \hat{\sigma}_{ij} = \frac{\sigma_{ij} L}{e_0 \phi_0} \quad \hat{\phi} = \frac{\phi}{\phi_0} \quad \hat{D}_i = \frac{D_i L C_0}{e_0^2 \phi_0} \quad (31)$$



**Figure 7.** Through-the-thickness distribution of (a) longitudinal stress, (b) transverse shear stress, (c) transverse normal stress, and (d) transverse electric displacement for a homogeneous axially poled PZT-5A clamped simply supported plate for the thermal load and length-to-thickness ratio  $S = 4$ .

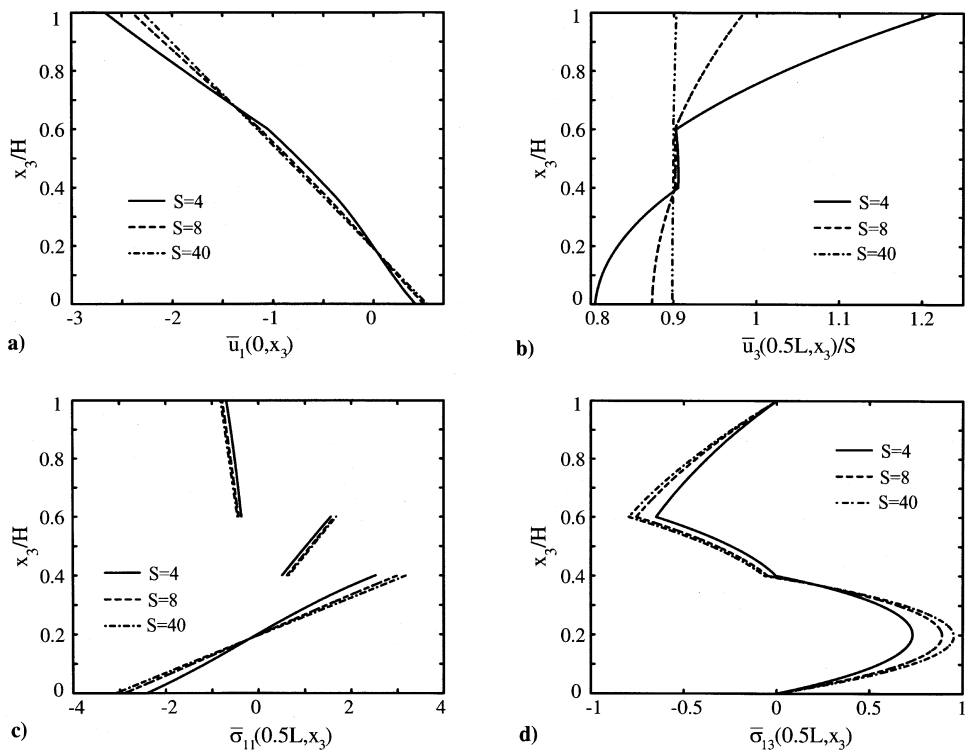
for the electrical load. The nondimensionalization parameters  $C_0$  and  $e_0$  are the same as those used earlier for the thickness poled piezoelectric materials.

Figure 7 evinces the through-the-thickness variation of the stresses and the longitudinal electric displacement for a clamped simply supported thick plate with  $S = 4$  and subjected to the thermal load. The longitudinal stress is a nonlinear function of  $x_3$ , especially in regions adjoining the clamped edge. The transverse shear stress profile is not parabolic at sections near the clamped edge due to the boundary layer effect there. The through-the-thickness variation of the transverse electric displacement  $\bar{D}_3$  is shown in Figure 7(d) at four locations along the span of the plate. The transverse shear and normal stresses for the electric load are shown in Figure 8. It is evident from Figure 8(a, b) that there are steep gradients in the stresses at the clamped edges. The transverse normal stress is intense within the boundary layer  $x_1 < 0.25L$  and essentially negligible at other locations. The through-the-thickness profile of the transverse shear stress is parabolic at the midspan and near the simply supported edge but deviates noticeably from the parabolic profile near the clamped edge.



**Figure 8.** Longitudinal variation of (a) transverse shear stress, and (b) transverse normal stress, and through-the-thickness variation of (c) transverse shear stress, and (d) transverse normal stress for a homogeneous axially poled PZT-5A clamped simply supported plate for the electric load and length-to-thickness ratio  $S = 4$ .

**Hybrid laminated plates.** A plate consisting of three layers with the bottom layer made of  $0^\circ$  Gr/Ep, the middle layer made of axially poled PZT-5A, and the top layer made of  $90^\circ$  Gr/Ep is considered next. Each Gr/Ep layer has thickness  $0.4H$  and the PZT-5A layer is of thickness  $0.2H$ . The top and bottom surfaces of the sandwiched PZT-5A layer are electrically grounded. The edges are free of electric charge and maintained at the reference temperature. Results for a simply supported plate that is subjected to the thermal load (28) are presented in Figure 9 for length-to-thickness ratios  $S = 4, 8$ , and  $10$ . The axial displacement profile in the thickness direction is a nonlinear function of  $x_3$  for thick plates, but it approaches an affine function for thin plates. The through-the-thickness variation of the transverse deflection is depicted in Figure 9(b). The transverse deflection is constant in the thickness direction for thin plates, but there is significant thickness distention for thick plates. The longitudinal stress, shown in Figure 9(c), is a piecewise affine function of the thickness coordinate for both thick and thin plates.



**Figure 9.** Through-the-thickness distribution of (a) axial deflection, (b) transverse deflection, (c) longitudinal stress, and (d) transverse shear stress for a laminated  $[0^\circ$  Gr/Ep, axially poled PZT-5A,  $90^\circ$  Gr/Ep] simply supported plate for the thermal load and length-to-thickness ratios  $S = 4, 8$ , and  $12$ .

## CONCLUSIONS

We have used the Eshelby–Stroh formalism to study the generalized plane strain deformations of multilayered thermopiezoelectric plates subjected to arbitrary thermal, electrical, and mechanical boundary conditions at the edges. The three-dimensional equations of quasi-static, linear thermopiezoelectricity simplified to the case of generalized plane strain deformations are exactly satisfied at every point in the body. The analytical solution is in terms of infinite series. The continuity conditions at the interfaces and boundary conditions on the bounding surfaces are used to determine coefficients in the series.

Results for a thermal load applied to the top surface of homogeneous and laminated piezoelectric plates poled in the thickness direction with clamped, traction-free, or simply supported edges have been presented. For a clamped simply supported plate, the stresses exhibit boundary layers at the clamped edges. The width of the boundary layers generally decreases for increasing length-to-thickness ratio. Results are also presented for homogeneous and piezoelectric plates that are poled in the axial direction.

The computed results prove the versatility of the proposed technique for obtaining accurate stresses for thick hybrid multilayered plates subjected to various thermal, electrical, and mechanical boundary conditions. The tabulated results presented herein should help ascertain the accuracy of various plate theories and finite element formulations.

## REFERENCES

1. M. D. Dunn, Micromechanics of Coupled Electroelastic Composites: Effective Thermal Expansion and Pyroelectric Coefficients, *J. Appl. Phys.*, vol. 73, pp. 5131–5140, 1993.
2. B. Jiang and R. C. Batra, Micromechanical Modeling of a Composite Containing Piezoelectric and Shape Memory Alloy Inclusions, *J. Intelligent Mat. Struct.*, vol. 12, pp. 165–182, 2001.
3. R. D. Mindlin, Equations of High Frequency Vibrations of Thermopiezoelectric Crystal Plates, *Int. J. Solids Struct.*, vol. 10, pp. 625–632, 1974.
4. W. Nowacki, Some General Theorems of Thermopiezoelectricity, *J. Thermal Stresses*, vol. 1, pp. 171–182, 1978.
5. D. Iesan, On Some Theorems in Thermopiezoelectricity, *J. Thermal Stresses*, vol. 12, pp. 209–223, 1989.
6. Y. N. Huang and R. C. Batra, A Theory of Thermoviscoelastic Dielectrics, *J. Thermal Stresses*, vol. 19, pp. 419–430, 1996.
7. J. S. Yang, Nonlinear Equations of Thermoviscoelectricity, *Math. Mech. Solids*, vol. 3, pp. 113–124, 1998.
8. T. R. Tauchert, Piezothermoelastic Behavior of a Laminated Plate, *J. Thermal Stresses*, vol. 15, pp. 25–37, 1992.
9. K. D. Jonnalagadda, G. E. Blandford, and T. R. Tauchert, Piezothermoelastic Composite Plate Analysis Using First-Order Shear-Deformation Theory, *Computers Struct.*, vol. 51, pp. 79–89, 1994.
10. S. S. Rao and M. Sunar, Analysis of Distributed Thermopiezoelectric Sensors and Actuators in Advanced Intelligent Structures, *AIAA J.*, vol. 31, pp. 1280–1286, 1993.
11. H. S. Tzou and R. Ye, Piezothermoelasticity and Precision Control of Piezoelectric Systems: Theory and Finite Elements Analysis, *J. Vibration Acoustics*, vol. 116, pp. 489–495, 1994.
12. Y. Y. Tang, A. K. Noor, and K. Xu, Assessment of Computational Models for Thermoelastoelectric Multilayered Plates, *Computers Structures*, vol. 61, pp. 915–933, 1996.

13. H.-J. Lee and D. A. Saravanos, Coupled Layerwise Analysis of Thermopiezoelectric Composite Beams, *AIAA J.*, vol. 34, pp. 1231–1237, 1996.
14. M. Ishihara and N. Noda, Piezothermoelastic Analysis of a Cross-Ply Laminate Considering the Effects of Transverse Shear and Coupling, *J. Thermal Stresses*, vol. 23, pp. 441–461, 2000.
15. G. P. Dube, S. Kapuria, and P. C. Dumir, Exact Piezothermoelastic Solution of Simply-Supported Orthotropic Flat Panel in Cylindrical Bending, *Int. J. Mech. Sci.*, vol. 38, pp. 1161–1177, 1996.
16. G. P. Dube, M. M. Upadhyay, P. C. Dumir, and S. Kumar, Piezothermoelastic Solution for Angle-Ply Laminated Plate in Cylindrical Bending, *Structural Eng. Mech.*, vol. 6, pp. 529–542, 1998.
17. S. Kapuria, G. P. Dube, and P. C. Dumir, Exact Piezothermoelastic Solution for Simply Supported Laminated Flat Panel in Cylindrical Bending, *Zeit. Angew. Math. Mech.*, vol. 77, pp. 281–293, 1997.
18. F. Shang, Z. Wang, and Z. Li, Analysis of Thermally Induced Cylindrical Flexure of Laminated Plates with Piezoelectric Layers, *Composites Pt. B*, vol. 28, pp. 185–193, 1997.
19. K. Xu, A. K. Noor, and Y. Y. Tang, Three-Dimensional Solutions for Coupled Thermoelastoelectric Response of Multilayered Plates, *Computer Methods Appl. Mech. Eng.*, vol. 126, pp. 355–371, 1995.
20. Y. Y. Tang and K. Xu, Dynamic Analysis of a Piezothermoelastic Laminated Plate, *J. Thermal Stresses*, vol. 18, pp. 87–104, 1995.
21. Y. Ootao and Y. Tanigawa, Three-Dimensional Transient Piezothermoelasticity for a Rectangular Composite Plate Composed of Cross-Ply and Piezoelectric Laminae, *Int. J. Eng. Sci.*, vol. 38, pp. 47–71, 2000.
22. Z. Q. Cheng and R. C. Batra, Three-Dimensional Asymptotic Scheme for Piezothermoelastic Laminates, *J. Thermal Stresses*, vol. 23, pp. 95–110, 2000.
23. F. Ashida and T. R. Tauchert, A General Plane-Stress Solution in Cylindrical Coordinates for a Piezothermoelastic Plate, *Int. J. Solids Struct.*, vol. 38, pp. 4969–4985, 2001.
24. J. S. Yang and R. C. Batra, Free Vibrations of a Linear Thermopiezoelectric Body, *J. Thermal Stresses*, vol. 18, pp. 278–295, 1995.
25. T. R. Tauchert, F. Ashida, N. Noda, S. Adali, and V. Verjzenko, Developments in Thermopiezoelectricity with Relevance to Smart Composite Structures, *Composite Struct.*, vol. 48, pp. 31–38, 2000.
26. J. D. Eshelby, W. T. Read, and W. Shockley, Anisotropic Elasticity with Applications to Dislocation Theory, *Acta Metal.*, vol. 1, pp. 251–259, 1953.
27. A. N. Stroh, Dislocations and Cracks in Anisotropic Elasticity, *Philos. Mag.*, vol. 3, pp. 625–646, 1958.
28. T. C. T. Ting, *Anisotropic Elasticity. Theory and Applications*, in *Oxford Engineering Science Series*, No 45. Oxford Univ. Press, New York, 1996.
29. S. S. Vel and R. C. Batra, Cylindrical Bending of Laminated Plates with Distributed and Segmented Piezoelectric Actuators/Sensors, *AIAA J.*, vol. 38, pp. 857–867, 2000.
30. S. S. Vel and R. C. Batra, Generalized Plane Strain Thermoelastic Deformation of Laminated Anisotropic Thick Plates, *Int. J. Solids Struct.*, vol. 38, pp. 1395–1414, 2001.
31. W. Nowacki, *Dynamic Problems of Thermoelasticity*, Noordhoff, Leyden, 1975.
32. D. L. Clements, Thermal Stress in Anisotropic Elastic Half-space, *SIAM J. Appl. Math.*, vol. 24, pp. 332–337, 1973.
33. Z. Suo, C.-M. Kuo, D. M. Barnett, and J. R. Willis, Fracture Mechanics for Piezoelectric Ceramics, *J. Mech. Phys. Solids*, vol. 40, pp. 739–765, 1992.
34. C. H. Wu, Plane Anisotropic Thermoelasticity, *J. Appl. Mech.*, vol. 51, pp. 724–726, 1984.
35. X. X. Yang, S. Shen, and Z. B. Kuang, The Degenerate Solution for Piezothermoelastic Materials, *European J. Mech. A, Solids*, vol. 16, pp. 779–793, 1997.
36. J. P. Dempsey and G. B. Sinclair, On the Stress Singularities in the Plane Elasticity of the Composite Wedge, *J. Elasticity*, vol. 9, pp. 373–391, 1979.
37. V. A. Boriseiko, V. S. Martynenko, and A. F. Ulitko, General Theory of Thin Piezoceramic Shells, *Vest. Kiev Univ. Mat. Mekh.*, vol. 25, pp. 26–40, 1983. (Ukrainian)
38. X. D. Zhang and C. T. Sun, Analysis of a Sandwich Plate Containing a Piezoelectric Core, *Smart Mat. Struct.*, vol. 8, pp. 31–40, 1999.
39. A. Benjeddou, M. A. Trindade, and R. Ohayon, A New Shear Actuated Smart Structure Beam Finite Element, *AIAA J.*, vol. 37, pp. 378–383, 1999.
40. S. S. Vel and R. C. Batra, Exact Solution for the Cylindrical Bending of Laminated Plates with Embedded Shear Actuators, *Smart Mat. Struct.*, vol. 10, pp. 240–251, 2001.

41. S. S. Vel and R. C. Batra, Exact Solution for Rectangular Sandwich Plates with Embedded Piezoelectric Shear Actuators, *AIAA J.*, vol. 39, pp. 1363–1373, 2001.
42. R. C. Batra and T. S. Geng, Comparison of Active Constrained Layer Damping by Using Extension and Shear Mode Piezoceramic Actuators, *J. Intelligent Mat. Struct.*, vol. 13, pp. 349–368, 2002.